## APPENDIX S1: MODEL DESCRIPTION

Here, we describe the environmental data and the growth model in more detail. The model Python code is publicly available in Zenodo, including all data and files required to run the model and generate the figures used in the main paper and here in the Appendix (see https://doi.org/10.5281/zenodo.4693460). Input data (temperature, prey fields, egg- and larval densities, data for plots) are embedded in the code or as separate files read into the model.

### Environmental data

*Bluefin tuna larvae.* We used data from bluefin tuna larvae (*Thunnus thynnus*) sampled during summer at the major spawning ground offshore the Balearic Island, Western Mediterranean in 2001-2013 - as described in Reglero et al. (2018). We added more recent samples from 2014-2017 (Alvarez-Berastegui et al. 2020) to find the spawning period (see grey bars in Figures 2B-C and Figure 3A in main text). The larval data correspond well with field data on eggs and gonad development (see Reglero et al. 2018) and shows that the spawning period is limited to a few weeks in June-July.

*Cladocera*. As our starting point, we use the monthly abundances of Cladocera collected during 1994-2003, with double oblique hauls from 0-70 m depth (Bongo net of 20 cm mouth diameter and mesh size of 250 mm). These data were collected on the shelf near the coast of Mallorca (Balearic Islands) and are published in Fernández De Puelles et al. (2007), while the ABFT spawning area is mainly further offshore from the Balearic Islands in the Western Mediterranean Sea (Reglero et al. 2012). This region is even more oligotrophic than the coastal area. Also, the

ABFT larvae only inhabit the upper 20 m of the water column (Reglero et al. 2018) while the zooplankton data in Fernández De Puelles et al. (2007) is averaged over 70 meters, and zooplankton vertical distribution is not uniform. We therefore scaled the average density with the vertical distribution pattern of Cladocera presented in Atienza et al. (2016) to find actual densities in the surface water where tuna larvae are found. We also interpolated the average monthly abundance estimates to daily values (Fig. S1).
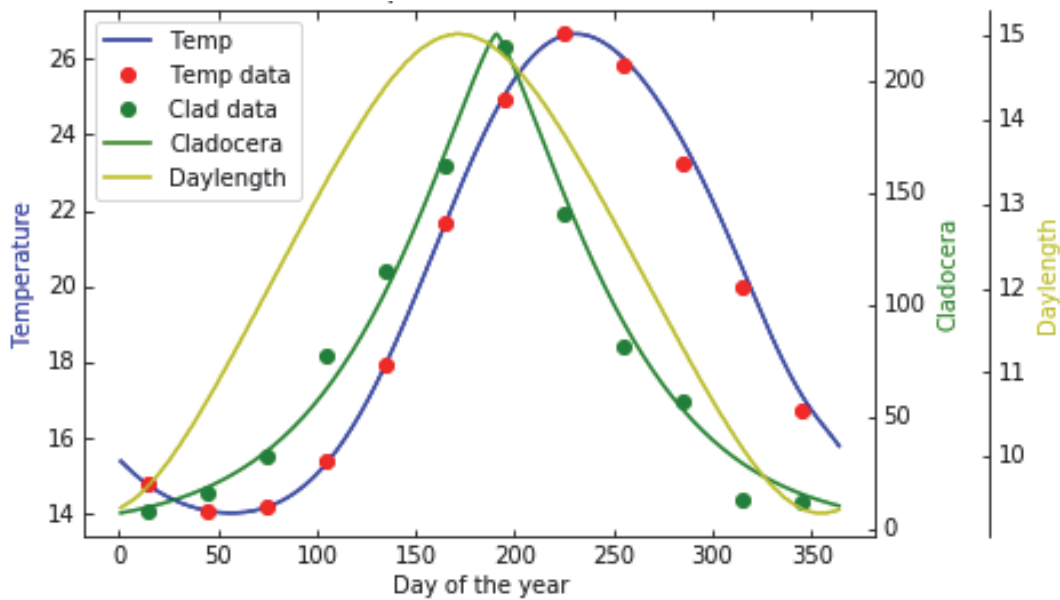


Figure S1. Seasonal cycles of environmental drivers. Surface temperature (ºC) where red dots are monthly means, blue line is interpolated daily values over the year from the NOAA CoastWatch Program and NASA's Goddard Space Flight Center (https://coastwatch.pfeg.noaa.gov/erddap/index.html) at tuna spawning areas near the Balearic Islands). Cladocera densities (# m$^{-3}$, green dots) are monthly averages from Fernández De Puelles et al. (2007) after scaling for vertical distribution with data from Atienza et al. (2016). The green line is fitted daily averages over the year (see text) near the surface in the Balearic Sea. Note that Cladocera densities decline further offshore, and the values used in the model sensitivity analysis is scaled down to 10-20% of these values, but the seasonal cycle is assumed to be the same. Also, nauplia prey densities remain stable over the season (see text). Daylength is the number of foraging hours available for the larvae (yellow line) over the year.

To interpolate to daily values for Cladocera densities, we fitted a modified Gaussian curve to the long-term mid-month data ($C_{day} = 220 * \exp(-0.5 * |(day - 190.8)/41.31|^{1.27})$), R$^2$ = 0.98), where $C_{day}$ is the number of Cladocera m$^{-3}$ and $day$ is the day of the year (1-365).

In general, open-ocean stations sampled across the Mediterranean Sea show lower abundance of all zooplankton groups than coastal stations (Berline et al. 2012). Samples collected above the thermocline in the tuna spawning area (Olivar et al. 2014, and own unpublished sampling, see Supplementary Table 1) do suggest that the concentration of Cladocera offshore is considerably less than near the shelf. This pattern fits well with what is seen along the Spanish mainland, where *Evadne* and *Pseudoevadne* became less abundant with increasing bottom depth (Atienza et al. 2016). Based on these observations we use baseline Cladocera densities of 10 - 20% of the monthly average measure at the coast, while we assume the seasonal abundance pattern is the same in the offshore area as near the coast.

Table S1. The average density (standard deviation in brackets) of *Evadne* and *Pseudoevadne* (Cladocera) and naupliae and copepodite sampled at the ABFT spawning ground off the Balearic Islands during June-July. For cladocera, a total of 38 stations were sampled using a Bongo-20 fitted with a net with a 250 microns mesh size equipped with flowmeters down to the thermocline. The sample was divided into two aliquots once onboard, one of them was preserved in 90% ethanol and further analyzed in the laboratory to count and identify Cladocera species. For naupliae and copepodite, a total of 19 stations were sampled using a Bongo-20 fitted with a net with a 55 microns mesh size equipped with flowmeters down to the thermocline. The whole sample was preserved in 90% ethanol was further analyzed in the laboratory to count nauplii and copepodites.

| Year | Number of stations | Mesh size (microns) | Depth strata | Group | Average density (± SD) |
|------|------|------|------|------|------|
| 2014 | 13 | 250 | 0-30 m | Cladocera | 22 (±29) |
| 2015 | 13 | 250 | 0-30 m | Cladocera | 66 (±84) |
| 2016 | 12 | 250 | 0-30 m | Cladocera | 4 (±6) |
| 2020 | 19 | 55 | 0-30 m | Nauplii | 267 (±151) |
| 2020 | 19 | 55 | 0-30 m | Copepodites | 248 (±157) |

*Copepod nauplii.* At first feeding, ABFT larvae feed mainly on smaller copepod nauplii, and gradually shift their diet towards Cladocera as they develop (Catalan et al. 2011). To find relevant densities of nauplii for the first feeding tuna larvae we have combined information from several studies: i) monthly depth-integrated abundances of nauplii sampled at the shelf near the Spanish

mainland (Calbet et al. 2001), and near the coast of Mallorca (de Puelles et al. 2003); ii) nauplii densities from some samples offshore near the bluefin tuna spawning areas in the Balearic Sea (Fernández De Puelles et al. 2014); iii) vertical distributions of nauplii and copepodites near the Spanish mainland (Sabatés et al. 2008, Olivar et al. 2010) and vertical distributions of copepods offshore the Balearic Sea (Olivar et al. 2014), iv) own sampling of nauplii and copepodites above the thermocline near the tuna spawning grounds during 2020 (Table S1).

Cladocera has a marked peak during summer, while monthly abundances of nauplii sampled on the shelf near the Spanish mainland and the coast of Mallorca remain nearly constant over the year (Calbet et al. 2001, de Puelles et al. 2003, Fernández de Puelles et al. 2007). Occasional sampling during summer in the spawning area offshore the Balearic Islands indicates the average density of nauplii integrated from 1 to 200 m depth reach a maximum of 1000 ind m$^{-3}$ (Fernández de Puelles et al. 2014, their figure 4). On the other hand, the vertical distribution of nauplii, copepodites and adults sampled at the Spanish mainland (Sabatés et al. 2008, Olivar et al. 2010) show that all these three life stages have peak densities deeper in the water column – near the chlorophyll maximum where the water is too cold for tuna larvae (Fig 1 A in main text). A few surveys offshore in the Balearic Sea have described similar vertical distribution patterns for adult copepods but do not include microzooplankton (Fernández de Puelles et al. 2014, Olivar et al. 2014). Based on net samples integrated over the upper 200 m (Calbet et al. 2001, de Puelles et al. 2003, Fernández de Puelles et al. 2014) and the vertical pattern described by Sabatés et al. (2008) and Olivar et al. (2010, 2014) we use values in the range 300-600 nauplii m$^{-3}$ near the surface throughout the season in our model. This is the range where most of the sensitivity to prey abundance appears in the model (see sensitivity analysis below), below this the larvae will starve and above they become satiated.

Zooplankton densities offshore the Balearic Islands are substantially lower than near the Spanish mainland further northwest, which adds to the question of why ABFT is spawning in

these oligotrophic areas. The review above show that nauplii-densities in the surface at the ABFT spawning area are low, and likely to be a limiting factor for growth at first feeding.

*Prey size.* The average length of the Cladocera prey is set to 0.8 mm (Catalán et al. 2007), and for the nauplii prey we use an intermediate value of 0.3 mm (typical size of *Oithona* nauplii). This prey was converted from length to mass using the expression $Log_{10}$ DW [micrograms dry mass] = -10.362+3.741$Log_{10}$ BL [body length in micrometres] in (Catalán et al. 2007) as estimated for *Evadne spinifera* resulting in a weight of 3.15 micrograms for a Cladocera and, from the expression in Hay et al. (1988) resulting in a weight of 0.5 micrograms dry mass for *Oithona* nauplii.

**The egg stage – development and survival.** In the model simulation, we release one egg every midnight since eggs tend to hatch during night time before 5 AM (Gordoa et al. 2009). We simulate a full annual cycle, but fitness of an egg outside day number 132-340 is zero, simply because they will not hatch in the cold water (Reglero et al. 2018). The chance of survival through the egg stage is determined by the daily mortality rate and the duration of the stage, driven by temperature (Fig. S2).

**The yolk sac stage.** After the egg hatches, the larva continues to develop its gut, vision and other organs before first feeding, based on energy from the yolk sac. We know that development through the yolk stage takes about 2.5 days at 25 degrees (Yúfera et al. 2014), but the exact temperature-dependency has not been measured. We assume a Q10 of 2, which makes temperature dependence of this stage duration similar to the egg stage, only a bit longer (Fig. S2).
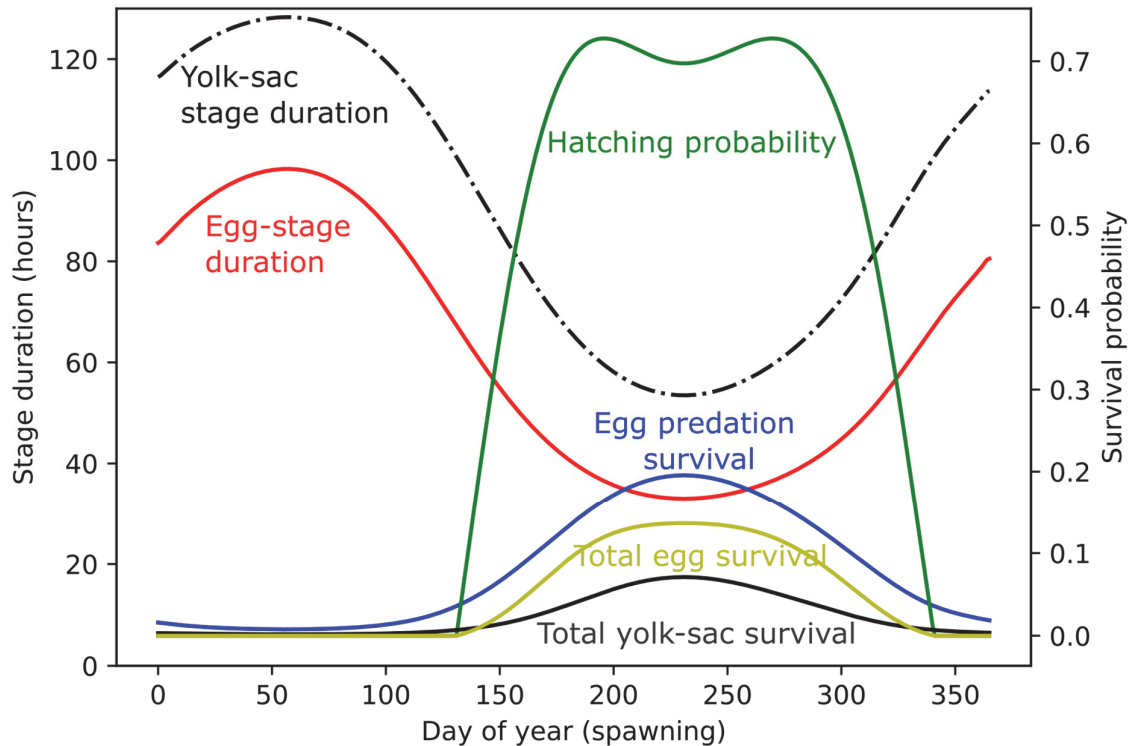
Figure S2. Egg hatching probability, development time, predation survival, and total survival chance; yolk-sac stage duration and survival of the yolk sac stage – all driven by the ambient temperature from day at hatching and onward. The small dip in hatching probability in mid-summer reflects that temperatures are higher than the optimum for a period. The size dependent mortality rate is assumed to be half of the rate in (McGurk 1986).

**The first feeding larva.** The larvae start feeding after the egg and yolk sac stage has been completed. Eggs are spawned at midnight, or at hour number 0 of the birthday, and will enter their first feeding stage at a time of the day purely determined by the temperature-dependent development rates. The larva starts first feeding at a body mass of 0.018 mg dry mass and complete the flexion larval stage when they reach 0.77 mg dry mass (Reglero et al. 2018).

The gut, including the stomach, is a dynamic flow-through state-variable in the model, similar to earlier models of larval cod (Fiksen and Jørgensen 2011, Fouzai et al. 2019). The amount of food in the gut is constrained to a fixed fraction of the body mass of the larva, based on measurements of gut content made in the lab (e. g. Blanco et al. 2017). The maximum dry mass of prey measured in the guts of ABFT is about 12% of the total dry body mass, with no

allometric pattern visible in the data (Blanco et al. 2017). Parts of this capacity may also be seen as energy and mass stored in metabolites in tissues and body fluids outside the gut. The storage capacity of the gut has consequences for how the larva maintain growth through the night when it does not feed (Catalan et al. 2011), or in a stochastic setting, how it copes with intermittency in feeding success. We know from intermittent feeding experiments that ABFT larvae grow slower if the interval between feeding or light periods become longer (Blanco et al. 2017), and this is captured within our model.

If the gut is not full, then encountered and successfully captured prey fill up the gut, and the dry mass required for growth and metabolic rate is drawn from the gut by digestion. If there is enough mass in the gut to sustain these rates, the larva grows by its temperature-dependent growth potential. The amount of dry mass $D$ required to grow at this rate is:

$$D = W(SGR_T + RMR_T)/\alpha \qquad \text{(Equation S1)}$$

where $SGR_T$ is the temperature-dependent specific growth rate (Reglero et al. 2018), $RMR_T$ is the resting metabolism (Blanco et al. 2020), $W$ is larval dry body mass and $\alpha$ is the assimilation efficiency (=0.77, see Reglero et al. 2011). If the gut contains less than $D$, all of it is used, and the body mass $W_h$ increase from one hour $h$ to the next according to the difference equation:

$$W_{h+1} = W_h + (\alpha G_h - W_h SMR_{T,h}). \qquad \text{(Equation S2)}$$

**Resting Metabolism (RMR).** Blanco et al. (2020) show that energy expenditure increases almost proportionally to the size of ABFT larvae: RMR=0.404 $W^{0.994}$, where RMR is measured in micromol $O_2$ hour$^{-1}$ at 26ºC and converted to milligrams of dry mass. We assume the temperature dependency of metabolism follows a $Q_{10} = 2$ (see Fig 1 in paper), a typical value for larval fish in general (Peck and Moyano 2016) including other tuna (Blank et al. 2007).

**Larval foraging model.** ABFT larvae are visual predators and search for prey during the day only (Catalan et al. 2011). The darkness itself limits search efficiency, particularly because the retina needs to develop before scotopic vision in low light is possible, and the development of rods take time (Hilder et al. 2019). We use Holling disk mechanics to model prey ingestion $i_{h,day}$ (mg DW h$^{-1}$) for every hour of the day through the year (see e.g. Varpe and Fiksen 2010):

$$i_{h,d,L} = \frac{P_c \beta_{C,h,d,L} C_d W_C}{1 + \tau \beta_{C,h,d,L} C_d} + \frac{\beta_{N,h,d,L} N W_N}{1 + \tau \beta_{N,h,day,L} N} . \text{(Equation S3)}$$

Here, $C_d$ is the density of Cladocera prey (# m$^{-3}$) at any given day of the year $d$ (Fig S1), $N$ is the density of copepod nauplii (400 m$^{-3}$, see above), $\tau$ is the handling time of each prey item (2 sec, but the encounter rate with Cladocera is low, so handling limitation only occurs for nauplii and at high abundance), $W_C$ (0.0015) and $W_N$ (0.0005) is the dry mass (in milligrams) of each of the two prey types and $P_c$ is the capture success of Cladocera prey. Based on diet data from the field, where no Cladocera is found in guts of first feeding larvae and few nauplii in larvae near flexion (Catalan et al. 2011), we let $P_c$ be a linear function from 0 at first feeding (0.018 mg DW larva) to 1 at flexion (0.77 mg DW larva).

The search rate $\beta_{h,d,L}$ (m$^3$ s$^{-1}$) depends mainly on the prey detection distance $R_L$ and the swimming speed of the larva:

$$\beta_{h,d,L} = \tfrac{1}{2} \pi R_L^2 v_L I_{h,d} \qquad \text{(Equation S4)}$$

The cruising velocity $v_L$ (m s$^{-1}$) was measured to three body lengths s$^{-1}$ in the lab (Reglero et al. 2015). The day-night periods are included as $I_{h,d}$ taking a value between 0 (night), 1 (daytime) or an interpolated value between at dusk and dawn. The factor ½ represent the fraction of the visual field that is effectively scanned, assuming larvae mainly look upwards and use the surface as background contrast to detect prey. This is supported by the high density of cells developing in the ventral retina of first feeding tuna larvae (Hilder et al. 2019).

The prey detection distance $R_L$ is an important variable here, as the volume searched per unit time is squared with $R_L$, and it effectively determines the search efficiency of the larva. Like many before us, we use the minimum separable angle (*MSA*), or visual acuity of the eye of a predator (e.g. Wanzenböck and Schiemer 1989, Job and Bellwood 1996, Caves et al. 2018) to model prey detection distance. The MSA depends on the size of the eye and the density of photoreceptors on the retina, which can be measured anatomically. In southern Bluefin tuna larvae, Hilder et al. (2019) recently measured *MSA* (in degrees) over the larval ontogeny, as a function of body length *L* in mm:

$$MSA = 4.699 L^{-1.129}. \qquad \text{(Equation S5)}$$

In daylight, MSA translates into visual detection distance $R_L$ as a function of prey length *H* and larval length from (for details, see Wanzenböck and Schiemer 1989, Job and Bellwood 1996, Caves et al. 2018):

$$R_L = \frac{0.5H}{\tan{(MSA/2)}}. \qquad \text{(Equation S6)}$$

The visual detection distance can be measured either behaviourally or anatomically, as we have done here. Comparisons of these two methods show that visual acuity and MSA is a theoretical maximum, and that the direct behavioural measure is typically about half as long for the same prey item (Job and Bellwood 1996, Parker et al. 2017). We therefore divide $R_L$ in Eq. S6 by 2 before use in Eq. S4.

**Mortality rate.** The default mortality rate of tuna eggs and larvae in this particular region has not been measured in the field, but one of the main hypotheses about spawning strategies in large, migratory predators like tuna is that they spawn in oligotrophic areas because there are few predators (Muhling et al. 2017). In our analysis, a higher level of mortality intensifies the reward of growing fast, which is recognized to be important to early life stages of fish (Bailey and Houde

1989, Fiksen and Jørgensen 2011, Fouzai et al. 2019). A lower rate of mortality punishes slow growth less than high mortality rates.

We take the review on mortality in fish eggs and larvae in general by McGurk (1986) as a starting point. He compiled many field estimates of daily mortality rate (M) and organized them as a function of larval fish of dry mass $W$ (in grams). Typically, mortality drops rapidly with body mass:

$$M_W = 2.2 \times 10^{-4} \times W^{-0.85} \text{ . (Equation S7)}$$

This model is mainly including species from more productive areas than in the oligotrophic areas where tuna spawn, like the Balearic Sea. One of the few field estimates of larval tuna mortality (Davis et al. 1991) followed a path of recently hatched larvae and estimated the mortality rate to 0.66 d$^{-1}$. This is considerably less than expected from the McGurk (1986) regression, so we have reduced our default value to half of Eq. S6.
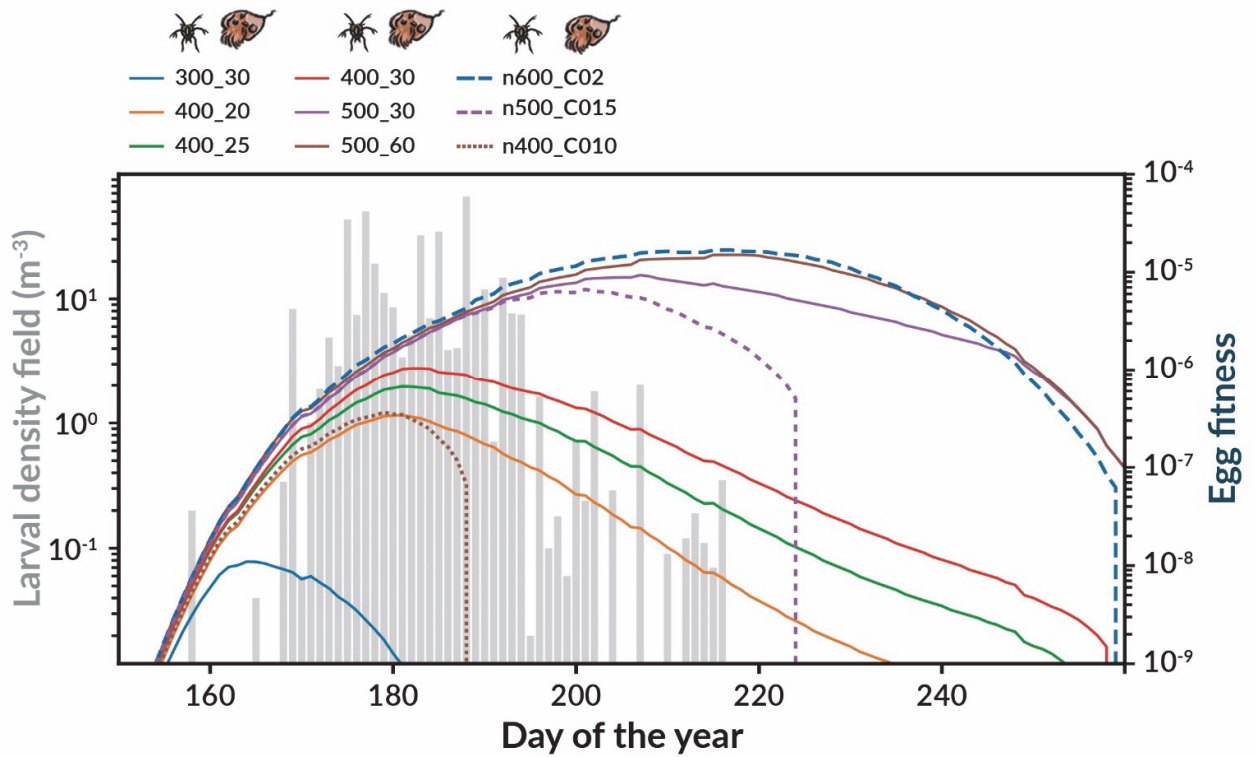
Figure S3. **Sensitivity of egg fitness over the season to different scenarios of nauplii and Cladocera abundance.** The lines show egg fitness if both nauplii and Cladocera concentrations are kept constant through the year, in combinations ranging from 300-500 nauplii and 10-60 Cladocera m$^{-3}$, or as 10-, 15, or 20% of the nearshore abundance (C010, C015, C02). The dotted and broken lines are the same as in Fig 3A in the paper, with a seasonal peak in Cladocera, but there they are scaled to their peak values to highlight the phenology consequences rather than the comparative survival effect. Note that it is the concentration of nauplii that comes out as the main driver of phenology (seen in the effect of 300-400-500 nauplii, at 30 Cladocera m$^{-3}$).
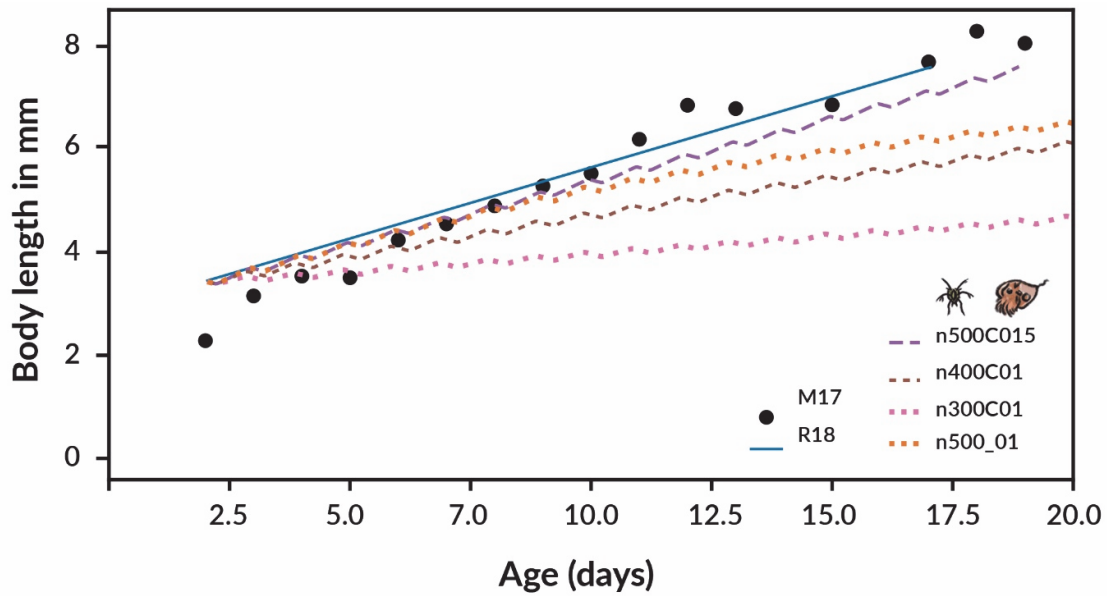
Figure S4. **Growth under different prey abundance in the model compared with growth in the lab and in the field.** The black dots (M17) are estimated growth from otolith increments in larvae from the field by Malca et al. (2017). The dotted and broken lines are model predictions under different prey concentrations, from 3-500 nauplii $m^{-3}$ and 10 (C01) or 15% (C015) of the long-term average coastal Cladocera (Fernández De Puelles et al. 2007). With 500 nauplii $m^{-3}$, 15% of Cladocera from coastal monitoring, and temperature and daylength at day 190, the larvae grow at rates comparable to estimates based on otoliths, but with fewer prey (400, 10%) growth is less than observed. The figure includes one simulation with 500 nauplii and 10 Cladocera $m^{-3}$ (n500_01) – to show how low abundance of Cladocera slows down growth in the later stages, but not younger ones.
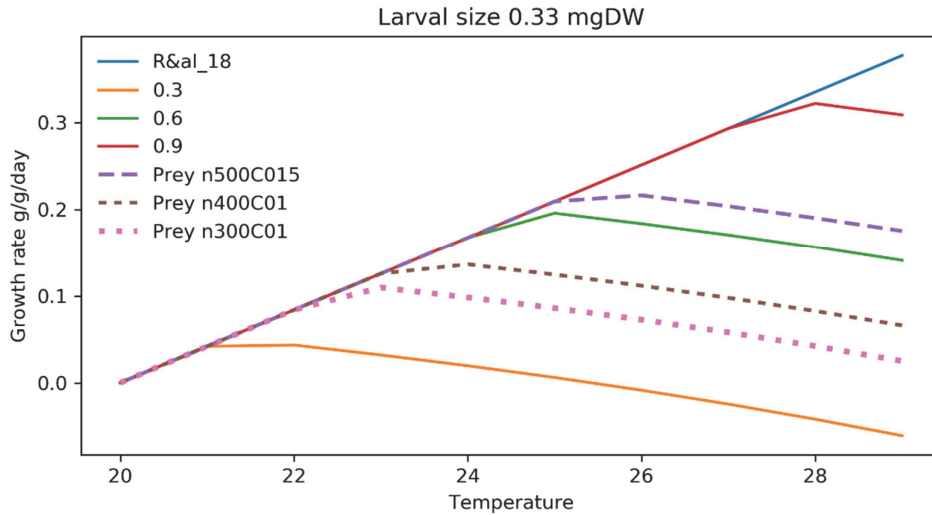
Figure S5. **A schematic picture of the metabolic meltdown**. The blue line is the temperature-dependent growth rate with no food limitation from Reglero et al. (2018). The other lines show specific growth rate (g $g^{-1}$ $day^{-1}$) if the larva can ingest fractions of 0.3, 0.6 or 0.9 of its body mass during a 15 hour day, only constrained by the gut size. The dotted lines are with the same prey concentrations as in the paper Figure 3 (300 +10%, 400+10% and 500 nauplii per $m^{-3}$ +15% of the nearshore Cladocera density, respectively. The example is for a 0.33 mg DW, or 6.6 mm larvae, with a mixed diet of nauplii and Cladocera. Note that the colours of the dotted lines match the prey combinations in Figs S4-S5.

**References in the online supplementary**

Alvarez-Berastegui, D., M. Tugores, D. Ottmann, M. Martín-Quetglas, and P. Reglero. 2020. Bluefin tuna larval indices in the western mediterranean, ecological and analytical sources of uncertainty. ICCAT Collective Volumes of Scientific Papers **77**:289-311.

Atienza, D., A. Sabatés, S. Isari, E. Saiz, and A. Calbet. 2016. Environmental boundaries of marine cladoceran distributions in the NW Mediterranean: Implications for their expansion under global warming. Journal of Marine Systems **164**:30-41.

Bailey, K. M., and E. D. Houde. 1989. Predation on eggs and larvae of marine fishes and the recruitment problem. Advances in Marine Biology **25**:1-83.

Berline, L., I. Siokou-Frangou, I. Marasović, O. Vidjak, M. L. Fernández de Puelles, M. G. Mazzocchi, G. Assimakopoulou, S. Zervoudaki, S. Fonda-Umani, A. Conversi, C. Garcia-Comas, F. Ibanez, S. Gasparini, L. Stemmann, and G. Gorsky. 2012. Intercomparison of six Mediterranean zooplankton time series. Progress in Oceanography **97-100**:76-91.

Blanco, E., P. Reglero, A. Ortega, F. De La Gándara, Ø. Fiksen, and A. Folkvord. 2017. The effects of light, darkness and intermittent feeding on the growth and survival of reared Atlantic bonito and Atlantic bluefin tuna larvae. Aquaculture **479**:233-239.

Blanco, E., P. Reglero, A. Ortega, A. Folkvord, F. de la Gandara, A. H. de Rojas, and M. Moyano. 2020. First estimates of metabolic rate in Atlantic bluefin tuna larvae. Journal of Fish Biology **97**:1296-1305.

Blank, J. M., J. M. Morrissette, C. J. Farwell, M. Price, R. J. Schallert, and B. A. Block. 2007. Temperature effects on metabolic rate of juvenile Pacific bluefin tuna *Thunnus orientalis*. Journal of Experimental Biology **210**:4254-4261.

Calbet, A., S. Garrido, E. Saiz, M. Alcaraz, and C. M. Duarte. 2001. Annual zooplankton succession in coastal NW Mediterranean waters: the importance of the smaller size fractions. Journal of Plankton Research **23**:319-331.

Catalán, I. A., F. Alemany, A. Morillas, and B. Morales-Nin. 2007. Diet of larval albacore *Thunnus alalunga* (Bonnaterre, 1788) off Mallorca Island (NW Mediterranean). Scientia Marina **71**:347-354.

Catalan, I. A., A. Tejedor, F. Alemany, and P. Reglero. 2011. Trophic ecology of Atlantic bluefin tuna *Thunnus thynnus* larvae. Journal of Fish Biology **78**:1545-1560.

Caves, E. M., N. C. Brandley, and S. Johnsen. 2018. Visual Acuity and the Evolution of Signals. Trends in Ecology & Evolution **33**:358-372.

Davis, T. L. O., V. Lyne, and G. P. Jenkins. 1991. Advection, dispersion and mortality of a patch of southern bluefin tuna larvae thunnus-maccoyii in the east-indian ocean. Marine ecology progress series **73**:33-45.

Fernández De Puelles, M. L., F. Alemany, and J. Jansá. 2007. Zooplankton time-series in the Balearic Sea (Western Mediterranean): Variability during the decade 1994–2003. Progress in Oceanography **74**:329-354.

Fernández De Puelles, M. L., V. Macias, L. Vicente, and J. C. Molinero. 2014. Seasonal spatial pattern and community structure of zooplankton in waters off the Baleares archipelago (Central Western Mediterranean). Journal of Marine Systems **138**:82-94.

Fiksen, Ø., and C. Jørgensen. 2011. Model of optimal behaviour in fish larvae predicts that food availability determines survival, but not growth. Marine ecology progress series **432**:207-219.

Fouzai, N., A. F. Opdal, C. Jørgensen, and Ø. Fiksen. 2019. Dying from the lesser of three evils: facilitation and non-consumptive effects emerge in a model with multiple predators. Oikos **128**:1307–1317.

Gordoa, A., M. P. Olivar, R. Arevalo, J. Vinas, B. Moli, and X. Illas. 2009. Determination of Atlantic bluefin tuna (*Thunnus thynnus*) spawning time within a transport cage in the western Mediterranean. ICES Journal of Marine Science **66**:2205-2210.

Hay, S. J., G. T. Evans, and J. C. Gamble. 1988. Birth, growth and death rates for enclosed populations of calanoid copepods. Journal of Plankton Research **10**:431-454.

Hilder, P. E., S. C. Battaglene, N. S. Hart, S. P. Collin, and J. M. Cobcroft. 2019. Retinal adaptations of southern bluefin tuna larvae: Implications for culture. Aquaculture **507**:222-232.

Job, S. D., and D. R. Bellwood. 1996. Visual acuity and feeding in larval Premnas biaculeatus. Journal of Fish Biology **48**:952-963.

Malca, E., B. Muhling, J. Franks, A. García, J. Tilley, T. Gerard, W. Ingram, and J. T. Lamkin. 2017. The first larval age and growth curve for bluefin tuna (*Thunnus thynnus*) from the Gulf of Mexico: Comparisons to the Straits of Florida, and the Balearic Sea (Mediterranean). Fisheries Research **190**:24-33.

McGurk, M. D. 1986. Natural mortality of marine pelagic fish eggs and larvae - role of spatial patchiness. Marine Ecology-Progress Series **34**:227-242.

Muhling, B. A., J. T. Lamkin, F. Alemany, A. García, J. Farley, G. W. Ingram, D. A. Berastegui, P. Reglero, and R. L. Carrion. 2017. Reproduction and larval biology in tunas, and the importance of restricted area spawning grounds. Reviews in Fish Biology and Fisheries **27**:697-732.

Olivar, M. P., M. Emelianov, F. Villate, I. Uriarte, F. Maynou, I. Álvarez, and E. Morote. 2010. The role of oceanographic conditions and plankton availability in larval fish assemblages off the Catalan coast (NW Mediterranean). Fisheries Oceanography **19**:209-229.

Olivar, M. P., A. Sabatés, F. Alemany, R. Balbín, M. L. Fernández De Puelles, and A. P. Torres. 2014. Diel-depth distributions of fish larvae off the Balearic Islands (western Mediterranean) under two environmental scenarios. Journal of Marine Systems **138**:127-138.

Parker, A. N., K. A. Fritsches, C. Newport, G. Wallis, and U. E. Siebeck. 2017. Comparison of functional and anatomical estimations of visual acuity in two species of coral reef fish. The Journal of Experimental Biology:jeb.149575.

Peck, M. A., and M. Moyano. 2016. Measuring respiration rates in marine fish larvae: challenges and advances. Journal in Fish Biology **88**:173-205.

de Puelles MF, Gras D, Hernandez-Leon S (2003) Annual cycle of zooplankton biomass, abundance and species composition in the neritic area of the Balearic Sea, Western Mediterranean. Marine Ecology 24:123–139

Reglero, P., L. Ciannelli, D. Alvarez-Berastegui, R. Balbin, J. L. Lopez-Jurado, and F. Alemany. 2012. Geographically and environmentally driven spawning distributions of tuna species in the western Mediterranean Sea. Marine ecology progress series **463**:273-+.

Reglero, P., A. Ortega, R. Balbin, F. J. Abascal, A. Medina, E. Blanco, F. de la Gandara, D. Alvarez-Berastegui, M. Hidalgo, L. Rasmuson, F. Alemany, and Ø. Fiksen. 2018. Atlantic bluefin tuna spawn at suboptimal temperatures for their offspring. Proceedings of the Royal Society B-Biological Sciences **285**:20171405.

Reglero, P., A. Urtizberea, A. P. Torres, F. Alemany, and Ø. Fiksen. 2011. Cannibalism among size classes of larvae may be a substantial mortality component in tuna. Marine ecology progress series **433**:205-219.

Reglero, P., N. Zaragoza, E. Blanco, F. de la Gandara, A. P. Torres, and A. Ortega. 2015. Routine swimming speed of bluefin tuna larvae measured in the laboratory. 39 Annual Larval Fish Conference, Vienna.

Sabates, A., N. Zaragoza, C. Grau, and J. Salat. 2008. Vertical distribution of early developmental stages in two coexisting clupeoid species, *Sardinella aurita* and *Engraulis encrasicolus*. Marine ecology progress series **364**:169-180.

Varpe, Ø., and Ø. Fiksen. 2010. Seasonal plankton-fish interactions: light regime, prey phenology, and herring foraging. Ecology **91**:311-318.

Wanzenböck, J., and F. Schiemer. 1989. Prey detection in cyprinids during early development. Canadian Journal of Fisheries and Aquatic Sciences **46**:995-1001.

Yúfera, M., J. B. Ortiz-Delgado, T. Hoffman, I. Siguero, B. Urup, and C. Sarasquete. 2014. Organogenesis of digestive system, visual system and other structures in Atlantic bluefin tuna (*Thunnus thynnus*) larvae reared with copepods in mesocosm system. Aquaculture **426-427**:126-137.